Gait Deviation Assessment: From Signal to Image Analysis

Lorenzo Hermez, Nesma Houmani, Sonia Garcia-Salicetti, Omar Galarraga, Vincent Vigneron

Gait Deviation Assessment: from Signal to Image Analysis

Lorenzo Hermez
SAMOVAR
Télécom SudParis, Institut Polytechnique de Paris
91120 Palaiseau, France
https://orcid.org/0009-0000-5974-9428

Nesma Houmani
SAMOVAR
Télécom SudParis, Institut Polytechnique de Paris
91120 Palaiseau, France
https://orcid.org/0000-0002-5048-9313

Sonia Garcia-Salicetti
SAMOVAR
Télécom SudParis, Institut Polytechnique de Paris
91120 Palaiseau, France
https://orcid.org/0000-0001-5257-8216

Omar Galarraga
Movement Analysis Laboratory
UGECAM Ile-de-France
77170 Coubert, France
https://orcid.org/0000-0002-5564-7624

Vincent Vigneron
Informatique, Bio-Informatique et Systèmes Complexes (IBISC) EA 4526
Université Paris-Saclay
91020 Evry, France
https://orcid.org/0000-0001-5917-6041

2024 IEEE Thirteenth International Conference on Image Processing Theory, Tools and Applications (IPTA) | 979-8-3315-4184-2/24/$31.00 ©2024 IEEE | DOI: 10.1109/IPTA62886.2024.10755780

***Abstract*—In this paper, we propose a novel framework for gait quality assessment based on image analysis, extending the traditional signal-based approach. Specifically, we construct Cycle Dissimilarity Images (CDI) from raw gait signals. Such images summarize all local dissimilarities existing in the dynamics between a gait signal and one normal gait reference. Also, we construct a typical dissimilarity image, by matching each normal gait reference to itself. Then, we propose to quantify gait deviations by computing the distance between the CDIs and the typical dissimilarity images. Our results indicate that, compared to the signal-based approach, this new framework leads to a more precise gait deviation assessment, and a more refined characterization of motor impairments, as hemiparesis, tetraparesis, and paraparesis.**

Keywords—clinical gait analysis, cycle dissimilarity image, normal gait reference image, dynamic time warping, deviation score, motor impairments.

I. Introduction

Human gait is a complex process that involves the coordination of multiple body segments and joints. In healthy individuals, this process is regulated by the Central Nervous System (CNS), which ensures the periodic movements of the limbs. However, neurological diseases such as cerebral palsy, multiple sclerosis, or stroke can cause CNS dysfunction, leading to impaired gait quality. The nature and extent of motor impairments due to these diseases can vary greatly depending on the pathology. In some cases, both upper and lower limbs may be affected simultaneously, as in paraparesis or tetraparesis. In other cases, only one side of the body may be impacted, as in hemiparesis.

In recent years, there have been significant advancements in the assessment of gait quality, thanks to the development of new technologies and research methodologies. Inertial measurement units [1-5] and motion capture systems [6,7] now enable the precise recording of kinematic joint angles [1, 8-11]. These recordings are used for clinical gait analysis to produce objective measurements that can assist clinicians in monitoring patients' progress and evaluating the effectiveness of interventions [12-14].

Different metrics have been proposed to quantify the deviations due to neurological diseases [15] from normal gait. The ability to accurately quantify these deviations is essential for the assessment of disease severity, the development of targeted rehabilitation strategies, and the evaluation of treatment efficiency. A few measures have been proposed in the literature for this purpose, including the Gait Deviation Index (GDI) [12], the Gait Profile Score (GPS) [13], and the Gillette Gait Index (GGI) [14].

The common method for creating a normal gait reference involves averaging the time-normalized gait cycles obtained from healthy individuals in a specific dataset, as proposed by the GPS [13]. Another approach is to create a universal gait feature space that includes both healthy and pathological subjects, and then average the vectors corresponding to healthy subjects within this space, as implemented by the GDI [12]. More recently, we have proposed a distance-based approach combined to unsupervised learning (*K*-Medoids) to retrieve *K* reference cycles that account for the intrinsic variability present in healthy gait [16]. Such reference cycles, called Normal Gait Profiles (NGPs), were retrieved using Dynamic Time Warping (DTW) distance to take advantage of raw (not normalized) gait signals. Then, to quantify pathological deviations from normal gait, we computed the DTW distance between a given cycle and the *K* NGPs, resulting in a *K*-dimensional deviation vector. Our method has been shown to outperform the state-of-the-art measures for quantifying pathological deviations [17].

This study proposes a new framework for evaluating gait deviations, switching from gait signal analysis to image analysis, following the same principles presented in [16]. More precisely, instead of computing deviations from normal gait on raw gait signals, we construct a Cycle Dissimilarity Image, carrying a comprehensive view of all the differences (local distances) existing in the dynamics between one Normal Gait Profile and one gait cycle. Indeed, such image leverages time shifts between a cycle and such reference, as well as their respective differences in amplitude.

Our approach also involves the creation of a Normal Gait Reference Image, by matching each Normal Gait Profile to itself. The assessment of gait deviation is carried out by comparing the Cycle Dissimilarity Image to the Normal Gait Reference Image using different metrics. Our results show that the proposed approach based on images outperforms our former results obtained on raw gait signals' analysis [16]. We demonstrate in the following the power of this novel framework for gait analysis.

The paper is organized as follows. In Section 2, we describe our dataset and the acquisition protocol, the process of creating the Cycle Dissimilarity Images, and the methodology employed to assess gait deviations using the

proposed images. Section 3 presents the results of our analysis, including a comparison of different metrics and with our previous state-of-the-art study. Finally, in Section 4, we offer our conclusions and discuss potential avenues for future research in this area.

II. Material and Methods

A. Data acquisition protocol and preprocessing

For this retrospective study, we used angular kinematic data of 52 healthy individuals and 45 patients with neurological diseases. The data was collected at the Movement Analysis Laboratory of Coubert Rehabilitation Center of UGECAM Ile-de-France, which is a healthcare institution specialized in neuromotor rehabilitation. Each participant was informed that his/her data might be used for research purposes, and no participant objected to the use of his/her data. This retrospective study was approved on April 10th, 2019, by the internal ethics committee of UGECAM Ile-de-France.

Data acquisition was performed during a spontaneous gait task using a Codamotion optoelectronic system integrating four CX1 cameras. The system was used to capture 3D angular kinematics of the pelvis, hip, foot, ankle, and knee in the sagittal, frontal, and transverse planes at a sampling rate of 100 Hz. Participants were instructed to walk naturally at a self-selected speed, for 10 meters in a straight line. This process was repeated five times in average, with each repetition constituting one gait trial.

The healthy control (HC) group consists of young adults aged 18 to 41 years who had no diseases affecting motor function. The patient group is composed of adults aged 21 to 75 years old (refer to Table I for more details). Among the 45 patients, 21 have hemiparesis (HP), 13 have incomplete tetraparesis (TP), and 11 have paraparesis (PP).

The angular kinematic signals of the joints were divided into gait cycles based on consecutive initial contact events. These events were automatically identified using a high-pass algorithm [21] and then manually verified by an expert. The number of gait cycles varied for each trial and patient. In total, the study dataset contains 526 HC, 200 HP, 98 PP and 126 TP gait cycles. Out of the 200 HP gait cycles, 100 cycles correspond to the affected lower limb and the remaining 100 cycles correspond to the non-affected lower limb.

For comparative purposes to our previous work [16], we focus this study only on the knee angular kinematics in the sagittal plane.

B. Recall on Normal Gait Profiles extraction

In our former work [16], to create a model of normal gait, we selected different representatives from the healthy population, called Normal Gait Profiles (NGPs). To achieve this, we applied an unsupervised algorithm called *K*-Medoids [22] on raw gait signals after a *kmeans++* initialization [23], coupled to an elastic distance, namely Dynamic Time Warping (DTW) [24].

TABLE I. Summary measures (Mean ± Standard Deviation) for healthy and pathological populations

	HC	***Patients***
Number of individuals	52	45
Number of gait cycles	526	424
Female	34 (65%)	14 (31%)
Age (years old)	22.61 ± 3.88	46.64 ± 12.7
Height (m)	1.71 ± 0.09	1.70 ± 0.1
Weight (kg)	65.28 ± 10.77	70.84 ± 13.3
Left cycle length (nb. points)	107.4 ± 6.7	220.5 ± 125.0
Right cycle length (nb. points)	107.3 ± 6.6	222.8 ± 131.9

DTW is suitable to align and compare two raw gait signals that may be of different length. It works by finding the optimal warping path that minimizes the cumulative distance between the corresponding points in the two signals X and Y, even if they are not perfectly aligned in time. The DTW distance is given by:

$$DTW_q(X,Y) = \min_{\pi \in A(X,Y)} \left(\sum_{(i,j)\in\pi} |X_i - Y_j|^q\right)^{\frac{1}{q}} \quad (1)$$

where $A(X,Y)$ is the set of all possible warping paths that satisfy the boundary conditions (*i.e.,* the first and last points of X and Y are aligned) and monotonicity (*i.e.*, the warping path does not go backwards in time). In this study, we set the value of q to 2. By using DTW, we can achieve a more accurate comparison between two signals, since it tolerates local distortions and temporal shifts that may exist between them.

Following the results of our experiments in [16], we consider in this study three NGPs to characterize normal gait.

C. Dissimilarity Image construction

As mentioned in the introduction, we propose a novel framework by switching from gait signal analysis to image analysis. We propose to construct a dissimilarity image matching two raw signals and containing the point-wise Euclidean distances computed between every observation in the first signal (a gait cycle) and every observation in the other one (see Fig. 1). The purpose of this transformation is to account for all potential alignments of the two raw signals, rather than relying only on the optimal path obtained through DTW as in [16].

Since we use non-normalized knee gait cycles, the obtained images have varying sizes. Therefore, we normalize them to a (64,64) dissimilarity image.

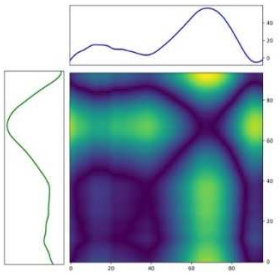

Fig. 1. Dissimilarity image constructed by comparing two raw gait cycles.

D. Gait quality assessment using Dissimilarity Images

To measure gait deviations based on such images, we adopt the following methodology:

1. We first extract the Normal Gait Profiles (NGPs) as explained in Section II.B.
2. We generate three Normal Gait Reference Images (NGRIs) constructed from the three NGPs (m_1, m_2, m_3) previously obtained. This is obtained by creating a dissimilarity image M_j (refer to Section II.C and Fig. 1) that matches each NGP cycle m_j to itself (see Fig. 2).
3. For a given cycle c_i (healthy or pathological) available in the database, we construct its corresponding Cycle Dissimilarity Image (CDI) by matching such cycle to each NGP. Therefore, three CDIs are obtained $CDI_{i,1}, CDI_{i,2}, CDI_{i,3}$ as illustrated in Fig. 3.
4. Then, for each cycle c_i, we compute a 3D deviation vector $D_i = [D_{i,1}, D_{i,2}, D_{i,3}]$ containing the distances between each CDI and each NRGI considering the metric d, namely:

$$D_{i,j} = d(CDI_{i,j}, M_j) \quad (2)$$

The metric d can be the Euclidean distance or the DTW distance. In next section, we explain how we compute the DTW distance between two images $CDI_{i,j}$ and M_j.

5. Finally, to assess gait deviation from normal gait, we apply Agglomerative Hierarchical Clustering on all the healthy and pathological cycles of the dataset represented by their 3D-vectors D_i (corresponding to each cycle c_i).

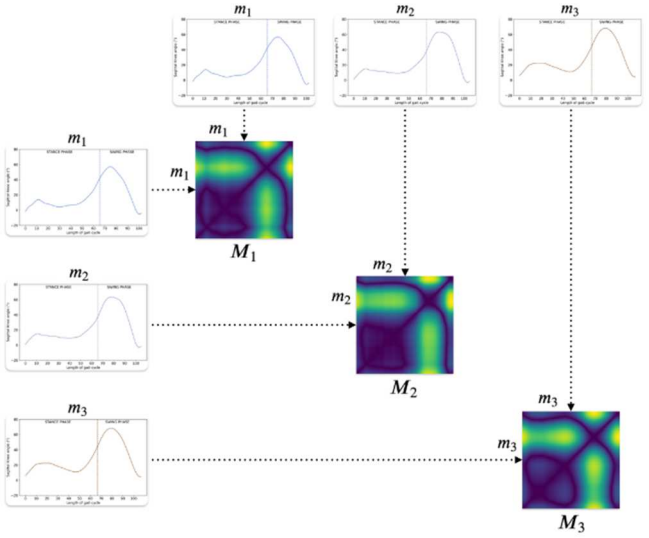

Fig. 2. Normal Gait References Images (NGRIs) constructed by matching each Normal Gait Profile (NGPs) to itself.

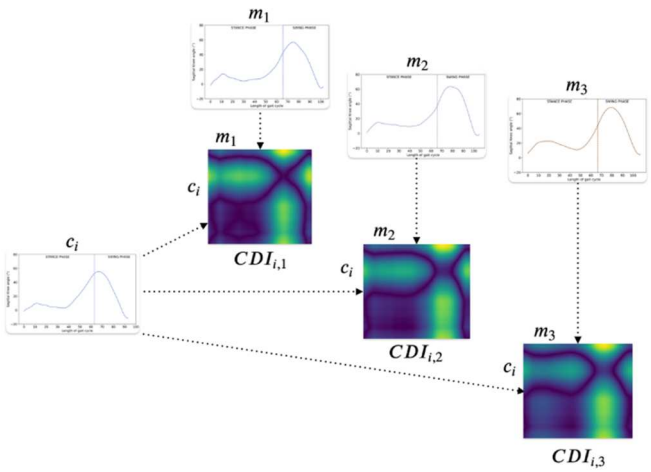

Fig. 3. Cycle Dissimilarity Images (CDIs) constructed by matching the cycle c_i to the three Normal Gait Profiles (NGPs).

E. Computing DTW distance between two dissimilarity images

To compute the DTW distance between the two images $CDI_{i,j}$ and M_j, we first construct a sequence of column vectors for each image. To this end, each image is split, from the left to the right, into a sequence of 64 column vectors of dimension 64. We thus obtain two sequences of vectors called Seq_1 and Seq_2.

To compute the DTW between both sequences, we calculate the local dissimilarity matrix with the Euclidean distance between each column vector $\boldsymbol{X}_i$ from Seq_1 to each column vector $\boldsymbol{Y}_j$ of Seq_2. The optimal path is searched in such dissimilarity matrix and the DTW distance is obtained as follows:

$$DTW(Seq_1, Seq_2) = \min_{\pi \in A(Seq_1, Seq_2)} \sum_{(i,j) \in \pi} \|\boldsymbol{X}_i - \boldsymbol{Y}_j\|^2 \quad (3)$$

where A is the set of all possible warping paths that satisfy the boundary conditions and monotonicity.

III. Experiments and Results

A. 3D clustering of deviation vectors computed with DTW

Fig. 4 displays the distribution of Cycle Dissimilarity Images (CDIs) of healthy controls and patients, into four clusters obtained with the hierarchical clustering. The clusters are displayed in green, dark green, orange and red, according to their progressive deviation from normal gait (NRGIs): the green cluster is the closest to normal gait, whereas the red cluster is the farthest.

We grouped the healthy controls to the left side and the patients by motor impairment (HP, PP and TP) to the right side. Each person is represented by a vertical bar counting the number of cycles assigned to each cluster.

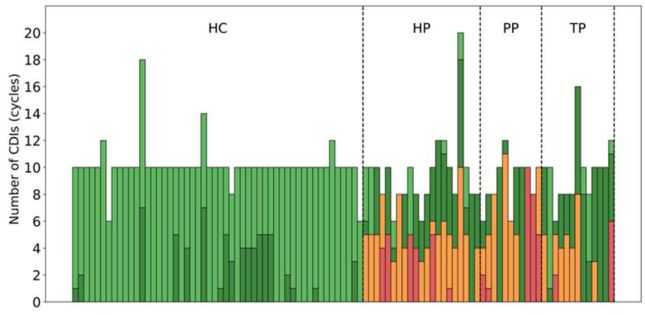

Fig. 4. Distribution of CDIs (cycles) for each person (a vertical bar) within the four clusters, based on DTW distance. CDIs in green are the closest to NGRIs, followed by CDIs in dark green, orange and red (the farthest to NGRIs). Persons are grouped per class: healthy controls (HC), Hemiparetic (HP), Paraparetic (PP) and Tetraparetic (TP) patients.

We first note that most HC cycles are assigned to the green cluster as expected, and the other HC cycles to the dark green cluster. On the other hand, pathological cycles are distributed on the four clusters in an explainable manner:

- For hemiparetic (HP) patients, we see a dominant trend of half of their cycles are assigned to one cluster (green or dark green), whereas the other half are assigned to another cluster (orange or red). This trend is observed for 19 HP patients among the 21. This accounts for the affected and non-affected sides of the body: the non-affected side cycles are found close to normal gait (green or dark green clusters) while the affected side cycles are found far from normal gait (orange or red clusters). Moreover, interestingly, we note that the non-affected side cycles are in majority assigned to the dark green cluster. This reflects the slight gait impairment of the non-affected side due to the compensation effects.
- For paraparetic (PP) patients, we observe the different trend: the cycles of each patient belong to only one cluster (dark green, orange or red). This is observed for 7 patients among the 11. We note that most cycles are assigned to the orange and red clusters, and there is no cycle assigned to the light green cluster. This accounts for the severity of motor impairments for both lower limbs in this group.
- For tetraparetic (TP) patients, compared to the PP group, we observe that more cycles are assigned to the dark green cluster and fewer cycles are assigned to the red one, showing that this class is less impaired. Also, we remark that 6 TP patients exhibit similar trend as HP: 5 TP have half of their cycles in the dark green cluster and half in the orange one; only one TP patient has half of his/her cycles in the dark green cluster and the other half in the red one.

These results show the effectiveness of our method in characterizing gait deviations from normal gait. Moreover, our method highlights the specific differences existing between motor impairments in the three patient groups.

We pursue our analysis by computing a scalar deviation score S_i for each cycle c_i, by averaging the three components of the 3D deviation vector D_i. Fig. 5 displays the deviation scores for each population. For the hemiparetic patients, we separated the affected (HPA) and non-affected (HPNA) sides.

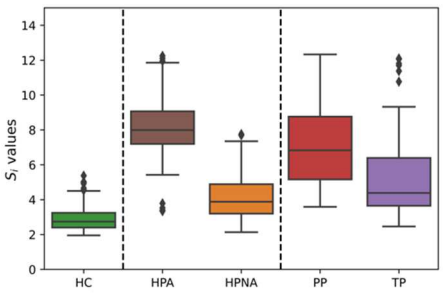

Fig. 5. Boxplots of the deviation scores for each class. HPA and HPNA stand respectively for HP patients' affected and non-affected sides.

The distinction between the affected (HPA) and non-affected (HPNA) sides in HP patients is highly significant, with a Mood's median test p-value of 5.6×10^{-29}. This result shows that our deviation score behaves well. We also note that for HC, the score values are the lowest and with low variance compared to patients. On the other hand, the boxplot for paraparetic patients is comparable to that of HPA in terms of score values (although a slight decrease of the median appears compared to HPA). Finally, the boxplot for tetraparetic patients is situated in between that of PP and HPNA.

B. 3D clustering of deviation vectors computed with Euclidean distance

We compare the results of our method when using the Euclidean distance versus DTW in Equation 2. Fig. 6 shows the distribution of Cycle Dissimilarity Images of healthy controls and patients, into four clusters, based on Euclidean distance. The clusters are displayed in the same color code as that of Fig. 4 for comparative purposes.

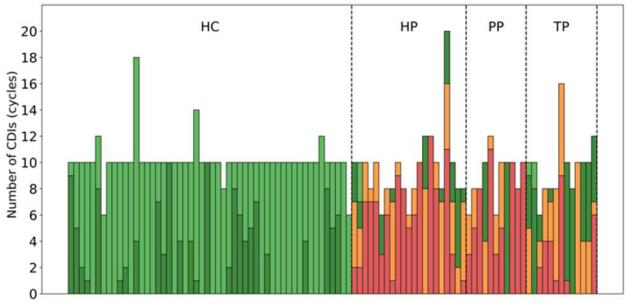

Fig. 6. Distribution of CDIs (cycles) for each person (a vertical bar) within the four clusters, based on Euclidean distance. CDIs in green are the closest to NGRIs, followed by CDIs in dark green, orange and red (the farthest to NGRIs). Persons are grouped per class: healthy controls (HC), Hemiparetic (HP), Paraparetic (PP) and Tetraparetic (TP) patients.

We observe that most pathological cycles are in the red cluster (the farthest from the NGRIs) contrary to the previous results obtained with DTW in Fig. 4. Also, with Euclidean distance, we no longer capture the specific trend previously observed in the HP class, distinguishing between affected and non-affected sides. This is shown more precisely in Fig. 7 displaying the distribution of deviation scores for HPA and HPNA, when considering in Equation (2) the Euclidean distance (Fig. 7 left) and DTW (Fig.7 right).

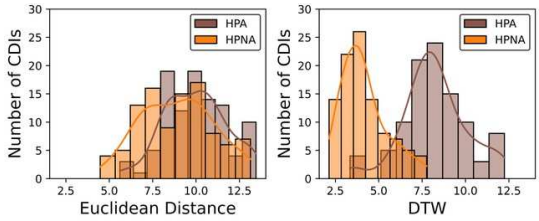

Fig. 7. Distribution of deviation scores obtained using the Euclidean distance (left) and the DTW (right) in Equation (2) for affected (HPA) and non-affected (HPNA) sides in hemiparetic patients.

All these results show that, contrary to DTW metric, using Euclidean distance in Equation (2) does not allow a refined characterization of motor impairment differences between the three patients' groups (HP, PP and TP).

C. *Image analysis versus raw signal analysis*

In our previous work [16], we emphasized the importance of exploiting different Normal Gait Profiles (NGPs) to account for the variability present in normal gait patterns. We compare in this section our approach based on images for gait analysis to the former one based on signal analysis.

Fig. 8 displays the results obtained with our former signal-based methodology. We remark that a high number of pathological cycles, especially in the PP class, belong to the dark green cluster, contrary to the image-based analysis (refer to Fig. 4). Nevertheless, the signal-based methodology seems to retrieve the same trend between affected and non-affected sides in HP (since cycles of both sides are often not assigned to the same cluster).

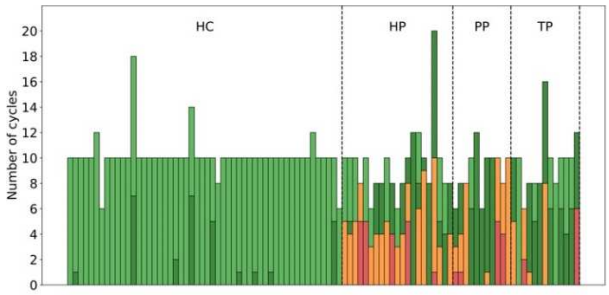

Fig. 8. Distribution of cycles for each person (a vertical bar) within the four clusters, with the signal-based approach of [16]. Cycles in green are the closest to NGPs, followed by cycles in dark green, orange and red (the farthest to NGPs). Persons are grouped per class: healthy controls (HC), Hemiparetic (HP), Paraparetic (PP) and Tetraparetic (TP) patients.

For deeper comparative analysis, we focus on the affected (HPA) and non-affected (HPNA) sides of hemiparetic patients. We consider the normalized deviation scores S_i computed on HPA and HPNA cycles. This score is computed for both approaches as the average of the three components in the 3D-vector associated to each cycle, when compared to the three normal gait references (NRGIs for the proposed image-based approach and NGPs for the signal-based approach [16]).

Fig. 9 and Fig. 10 respectively show the distributions of deviation scores for left and right cycles for each hemiparetic patient, when considering our image-based approach on one hand and the signal-based approach on the other hand.

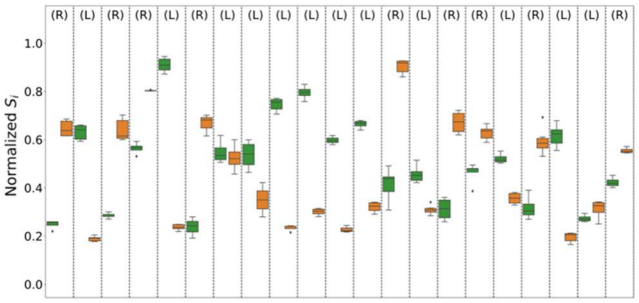

Fig. 9. Boxplots of deviation scores for left (in green) and right (in orange) cycles per HP patient (one column), considering the image-based approach. The affected side is indicated by "L" (left) or "R" (right) at the top for each patient.

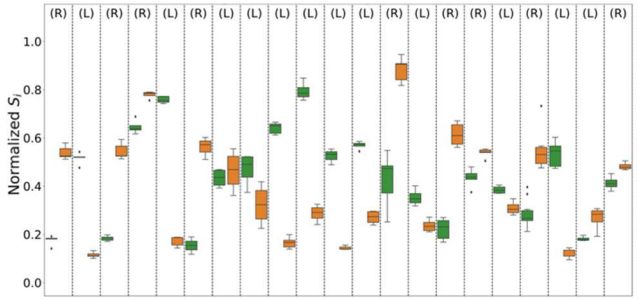

Fig. 10. Boxplots of deviation scores for left (in green) and right (in orange) cycles per HP patient (one column), considering the signal-based approach. The affected side is indicated by "L" (left) or "R" (right) at the top for each patient.

It can be seen that the separation between the affected and non-affected sides' score values is higher when performing the image-based analysis (Fig.9), as observed for the 4th, 5th, 8th, 13th, 14th, 17th, 18th, 19th, 21st hemiparetic patients.

Additionally, with the image-based approach, for all HP patients except one (patient 20), the affected side is correctly detected, since it has a higher score (this corresponds to higher values of the 3 distances in the deviation vector). For the signal-based approach (Fig.10), the affected side is wrongly detected in two cases (patients 7 and 20).

Finally, by performing the Mood's median test on the normalized deviation scores S_i computed on HPA and HPNA with the signal-based approach, we found a significant difference between HPA and HPNA cycles' scores, but with a much higher p-value of 2.7×10^{-21} than that obtained with our proposed image-based approach (5.6×10^{-29}). This difference reflects the higher precision of the image-based approach here proposed and its potential for further works in gait analysis.

IV. Discussion and Conclusion

In this study, we proposed a novel framework for gait analysis exploiting specific images constructed from raw gait signals. We first introduced images summarizing all the possible local dissimilarities existing in the dynamics between one gait cycle and one normal gait reference or "Normal Gait Profile" (NGP); such images are called "Cycle Dissimilarity Images" (CDIs). We kept to this end three representatives for normal gait (NGPs) to well represent the existing variability among the healthy population. We then introduced the "typical" dissimilarity image for each normal gait reference (namely "Normal Gait Reference Images" or NRGIs), generated by computing the local distances between each NGP and itself. We proposed to measure the deviations

between the former (CDIs) and the latter (NRGIs) to better characterize pathological gait deviations comparatively to our former work exploiting gait signals [16].

Results demonstrate that our image-based approach outperforms our former signal-based one, which was already shown to be a better way to quantify deviations compared to the well-known GDI and GPS [17]. Indeed, CDIs allow for a more detailed spatio-temporal representation of gait deviations, and thus a more precise assessment of motor impairments. More precisely, for HP patients, our results showed that a more accurate detection of the affected side is obtained with our proposed approach. Additionally, the gap between deviation scores for the affected (HPA) and non-affected (HPNA) sides in HP patients, is greater with CDIs compared to raw gait cycles, as displayed in Fig. 9 and Fig. 10, and confirmed by a much lower p-value of the Mood's test (a factor of 2×10^{-8}). This proves the effectiveness of our proposed images to differentiate gait quality of the affected and non-affected sides of the body.

Also, the image-based approach allows a more refined characterization of each patient group, when clustering the deviation vectors into four clusters. With the signal-based approach, a high number of PP cycles belongs to the dark green cluster, contrary to the image-based analysis (refer to Fig. 4) in which a more nuanced trend appears: most PP cycles are assigned to the orange and red clusters, accounting for the severity of motor impairments for both lower limbs.

The use of the DTW also showed significant improvements in quantifying gait deviations compared to the use of Euclidean distance. This is due to the fact that DTW can manage spatio-temporal shifts.

In conclusion, the proposed approach relying on images offers a comprehensive view of local differences existing in time and amplitudes between two raw gait signals. This contributes to describe gait in a higher-dimensional space allowing for a complete view of gait deviations. This novel perspective extends and outperforms the method in [16] and opens new possibilities for future work.

There are still some limitations to consider. The current study was conducted on a dataset of young healthy adults, which may not fully represent normal gait. Additionally, the number of patients per motor impairment was limited and there was an imbalance between groups. This highlights the need to conduct the study on an extended dataset to confirm our findings. Finally, other joints will also be considered in future works.

ACKNOWLEDGMENT

We thank Institut Mines-Telecom and Telecom SudParis for funding this research.

REFERENCES

[1] M. Błażkiewicz, A. Wit, 2018. Artificial neural network simulation of lower limb joint angles in normal and impaired human gait. Acta of bioengineering and biomechanics. 20 : 43–49.

[2] T.P. Luu, K.H. Low, X. Qu, H.B. Lim, K.H. Hoon, 2014. An individual-specific gait pattern prediction model based on generalized regression neural networks. Gait & posture. 39 : 443–448.

[3] S. Sivakumar, A.A. Gopalai, K.H. Lim, D. Gouwanda, 2019. Artificial neural network based ankle joint angle estimation using instrumented foot insoles. Biomedical Signal Processing and Control, 54, 101614.

[4] M.S. Renani, A.M. Eustace, C.A. Myers, C.W. Clary, 2021. The use of synthetic imu signals in the training of deep learning models significantly improves the accuracy of joint kinematic predictions. Sensors, 21, 5876.

[5] B.J. Stetter, F.C. Krafft, S. Ringhof, T. Stein, S. Sell, 2020. A machine learning and wearable sensor based approach to estimate external knee flexion and adduction moments during various locomotion tasks. Frontiers in bioengineering and biotechnology. **8**, 9.

[6] G. Giarmatzis, E. I. Zacharaki, K. Moustakas, "Real-time prediction of joint forces by motion capture and machine learning", Sensors, vol. 20, 6933, 2020.

[7] F. J. Wouda, M. Giuberti, G. Bellusci, P. H. Veltink, "Estimation of full-body poses using only five inertial sensors: an eager or lazy learning approach?", Sensors, vol. 16, 2138, 2016.

[8] R. Argent, S. Drummond, A. Remus, M. O'Reilly, B. Caulfield, "Evaluating the use of machine learning in the assessment of joint angle using a single inertial sensor", Journal of rehabilitation and assistive technologies engineering, vol. 6, 2019.

[9] J. Chen, X. Zhang, Y. Cheng, N. Xi, "Surface emg based continuous estimation of human lower limb joint angles by using deep belief networks", Biomedical Signal Processing and Control, vol. 40, pp. 335–342, 2018.

[10] S. Farmer, B. Silver-Thorn, P. Voglewede, S. A. Beardsley, "Within-socket myoelectric prediction of continuous ankle kinematics for control of a powered transtibial prosthesis", Journal of neural engineering, vol. 11, 056027, 2014.

[11] A. Findlow, J. Y. Goulermas, C. Nester, D. Howard, L. P. J Kenney, "Predicting lower limb joint kinematics using wearable motion sensors", Gait & posture, vol. 28, pp. 120–126, 2008.

[12] M. H. Schwartz, A. Rozumalski, "The gait deviation index: a new comprehensive index of gait pathology", Gait Posture, vol. 28, pp. 351–357, 2008.

[13] R. Baker, J. L. McGinley, M. H. Schwartz, et al., "The gait profile score and movement analysis profile", Gait Posture, vol. 30, pp. 265–269, 2009.

[14] A. Cretual, K. Bervet, L. Ballaz, "Gillette gait index in adults", Gait Posture, vol. 32, pp. 307–310, 2010.

[15] V. Cimolin, M. Galli, "Summary measures for clinical gait analysis: a literature review", Gait Posture, vol. 39, pp. 1005–1010, 2014.

[16] L. Hermez, A. Halimi, N. Houmani, et al., "Clinical gait analysis: characterizing normal gait and pathological deviations due to neurological diseases", Sensors, vol. 23, 6566, 2023.

[17] L. Hermez, N. Houmani, S. Garcia-Salicetti, O. Galarraga, V. Vigneron, "Gait deviation and neurological diseases: a comparative study of quantitative measures", IEEE E-Health and Bioengineering, November 2023, Bucharest, Romania.

[18] S. Sivapalan, D. Chen, S. Denman, S. Sridharan and C. Fookes, "Gait energy volumes and frontal gait recognition using depth images," 2011 International Joint Conference on Biometrics (IJCB), Washington, DC, USA, pp. 1-6, 2011.

[19] C. Wang, J. Zhang, J. Pu, X. Yuan, L. Wang, "Chrono-Gait Image: A Novel Temporal Template for Gait Recognition", In ECCV 2010, vol 6311, 2010.

[20] T. H. W. Lam, K .H. Cheung, J. N. K. Liu, "Gait flow image: A silhouette-based gait representation for human identification", Pattern Recognition, vol. 44, pp. 973-987, 2011.

[21] E. Desailly, Y. Daniel, P. Sardain, P. Lacouture, "Foot contact event de- tection using kinematic data in cerebral palsy children and normal adults gait", Gait Posture, vol. 29, pp. 76–80, 2009.

[22] L. Kaufman, "Partitioning around medoids (program pam)", Finding groups in data, vol. 344, pp. 68-125, 1990.

[23] D. Arthur & S. Vassilvitskii, "K-Means++: The Advantages of Careful Seeding", Proc. of the Annu. ACM-SIAM Symp. on Discrete Algorithms, vol. 8, pp. 1027-1035, 2007.

[24] H. Sakoe, S. Chiba, "Dynamic programming algorithm optimization for spoken word recognition", IEEE Transactions on Acoustics, Speech, and Signal Processing, vol. 26, pp. 43–49, 1978.

[25] J. H. Ward Jr, "Hierarchical grouping to optimize an objective function", Journal of the American statistical association, vol. 58, pp. 236-244, 1963.